Article

Electrical Behavior of Droplet Interface Bilayer Networks: Experimental Analysis and Modeling

William L. Hwang, Matthew A. Holden, Steven White, and Hagan Bayley

J. Am. Chem. Soc., **2007**, 129 (38), 11854-11864• DOI: 10.1021/ja074071a • Publication Date (Web): 01 September 2007

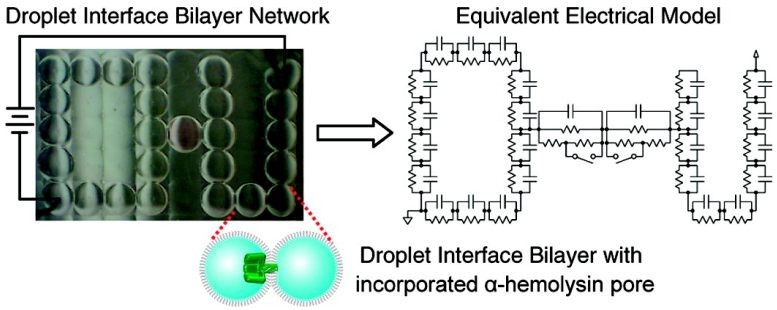

More About This Article

Additional resources and features associated with this article are available within the HTML version:

- Supporting Information
- Links to the 5 articles that cite this article, as of the time of this article download
- Access to high resolution figures
- Links to articles and content related to this article
- Copyright permission to reproduce figures and/or text from this article

View the Full Text HTML

J|A|C|S
ARTICLES
Published on Web 09/01/2007

Electrical Behavior of Droplet Interface Bilayer Networks: Experimental Analysis and Modeling

William L. Hwang,*,† Matthew A. Holden,† Steven White,‡ and Hagan Bayley†

Contribution from the Department of Chemistry, University of Oxford, Chemistry Research Laboratory, OX1 3TA, England, U.K., and Oxford NanoLabs Ltd., Begbroke Science Park, OX5 1PF, England, U.K.

Received June 5, 2007; E-mail: william.hwang@chem.ox.ac.uk

Abstract: Aqueous droplets submerged in an oil−lipid mixture become enclosed by a lipid monolayer. The droplets can be connected to form robust networks of droplet interface bilayers (DIBs) with functions such as a biobattery and a light sensor. Such DIB networks might be used as model systems for the study of membrane-based biological phenomena. In this study, we develop and experimentally validate an electrical modeling approach for DIB networks by applying it to describe the current flow through a simple network containing protein pores and blocking molecules. We demonstrate the use of SPICE (Simulation Program with Integrated Circuit Emphasis) for simulating the electrical behavior of DIB networks. The modular and scalable nature of DIB networks should enable a straightforward extension of the analysis presented in this paper to large, complex networks.

Introduction

The spontaneous formation of lipid bilayers at the interface between lipid monolayer-coated aqueous droplets has recently been demonstrated[1,2] and has several advantages over planar bilayers,[3] including increased lifetime and stability. In this technique, two aqueous droplets are submerged in an oil−lipid mixture. After the droplets become encased by lipid monolayers, they are brought into contact to form a long-lasting, robust droplet interface bilayer (DIB).[2] Linear and branched chains of droplets can be arranged to form large DIB networks.[2] The incorporation of ion channels and pores into DIBs enables measurement of ion currents through one or more interfaces via electrodes inserted into the droplets. Functional networks are created through the inclusion of membrane proteins with specific properties. For example, a three-droplet "biobattery" network can be designed by coupling an ionic gradient with α-hemolysin (αHL) pores engineered to be moderately anion-selective.[2] Bacteriorhodopsin, a light-activated proton pump, can be incorporated into DIB networks to create light-sensitive devices.[2]

Droplet interface bilayers are significantly more robust and long-lived by comparison with planar bilayers. DIBs can be separated and reformed multiple times by disconnecting and reconnecting droplets. In fact, a single droplet containing a membrane protein of interest can be scanned along a series of droplets containing various analytes as a low volume, high-throughput screening approach for membrane proteins.[2] Furthermore, the properties of a DIB network can be altered by excising and replacing individual droplets with droplets of different compositions.

Droplets in a DIB network can act as artificial "protocells" that communicate through bilayer-incorporated proteins. Artificial protocells have been designed to perform biological functions ranging from gene transcription[4−6] and protein synthesis[7] to energy production and storage.[8−10] Functional networks assembled from such protocells hold promise as a platform for modeling and studying membrane-based phenomena in biological systems. However, further study on the electrical properties of such networks is needed.

In this paper, we chose to investigate DIB networks containing wild-type αHL pores because they insert efficiently into DIBs,[2] are well-characterized,[11] and can be engineered to have diverse functions.[12] Moreover, αHL pores adopt a known orientation in a bilayer,[11,13] which means that the location of protein domains can be controlled by the arrangement of droplets. We show that DIB networks exhibit electrical phenomena that are not observed in single bilayers, which need

† University of Oxford.
‡ Oxford NanoLabs Ltd.

(1) Funakoshi, K.; Suzuki, H.; Takeuchi, S. *Anal. Chem.* **2006**, *78*, 8169−8174.
(2) Holden, M. A.; Needham, D.; Bayley, H. *J. Am. Chem. Soc.* **2007**, *129*, 8650−8655.
(3) Montal, M.; Mueller, P. *Proc. Natl. Acad. Sci. U.S.A.* **1972**, *69*, 3561−3566.
(4) Fischer, A.; Franco, A.; Oberholzer, T. *ChemBioChem* **2002**, *3*, 409−417.
(5) Luisi, P. L.; Ferri, F.; Stano, P. *Naturwissenschaften* **2006**, *93*, 1−13.
(6) Noireaux, V.; Bar-Ziv, R.; Godefroy, J.; Salman, H.; Libchaber, A. *Phys. Biol.* **2005**, *2*, P1−P8.
(7) Pietrini, A. V.; Luisi, P. L. *ChemBioChem* **2004**, *5*, 1055−1062.
(8) Bennett, I. M.; Farfano, H. M. V.; Bogani, F.; Primak, A.; Liddell, P. A.; Otero, L.; Sereno, L.; Silber, J. J.; Moore, A. L.; Moore, T. A.; Gust, D. *Nature* **2002**, *420*, 398−401.
(9) Bhosale, S.; Sisson, A. L.; Talukdar, P.; Furstenberg, A.; Banerji, N.; Vauthey, E.; Bollot, G.; Mareda, J.; Roger, C.; Wurthner, F.; Sakai, N.; Matile, S. *Science* **2006**, *313*, 84−86.
(10) Luo, T. J. M.; Soong, R.; Lan, E.; Dunn, B.; Montemagno, C. *Nat. Mater.* **2005**, *4*, 220−224.
(11) Song, L. Z.; Hobaugh, M. R.; Shustak, C.; Cheley, S.; Bayley, H.; Gouaux, J. E. *Science* **1996**, *274*, 1859−1866.
(12) Bayley, H.; Jayasinghe, L. *Mol. Membr. Biol.* **2004**, *21*, 209−220.
(13) Gouaux, E. *J. Struct. Biol.* **1998**, *121*, 110−122.

10.1021/ja074071a CCC: $37.00

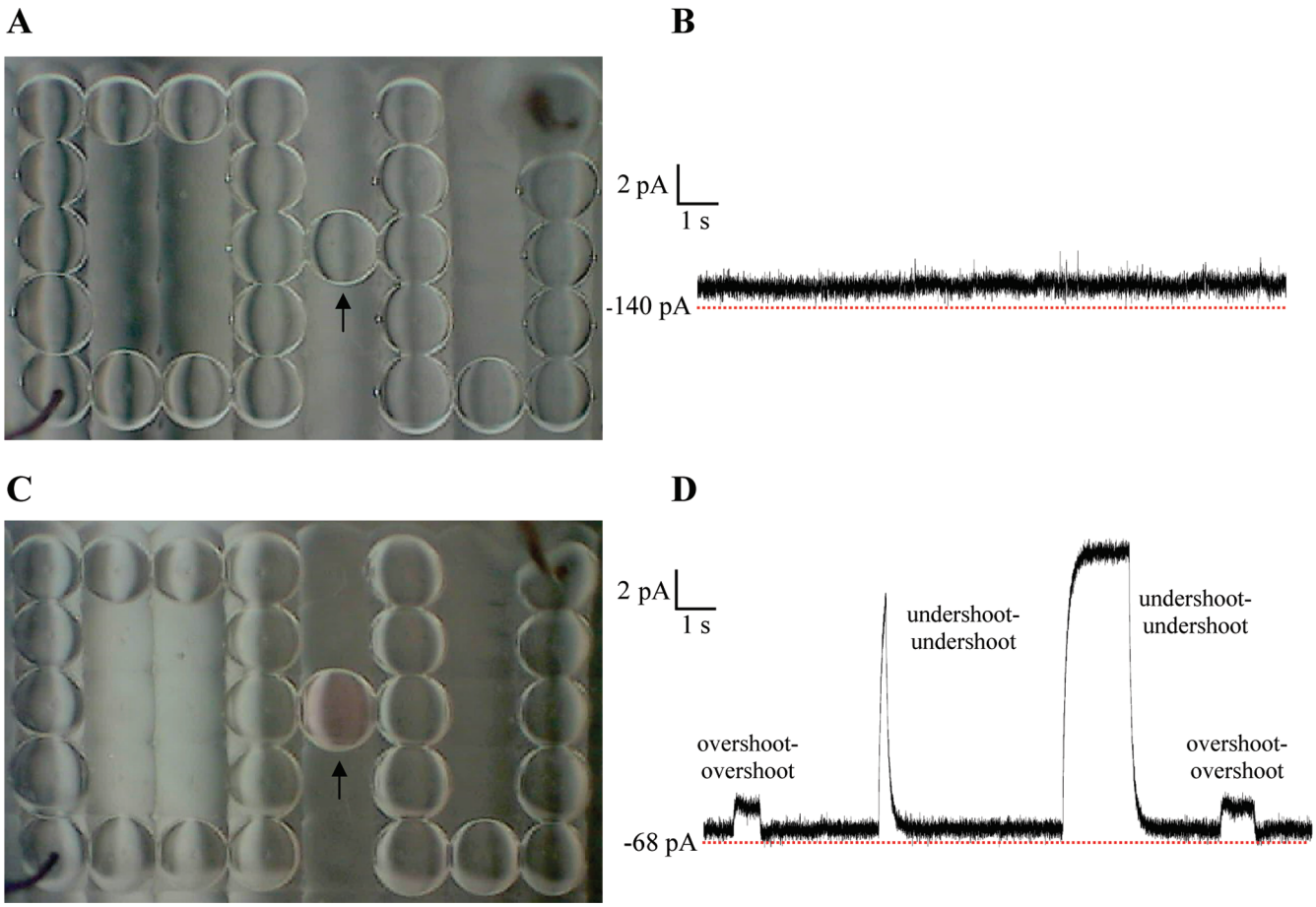

Figure 1. "O−U" droplet interface bilayer network. (A) 26-droplet DIB network in the form of an "O−U." Each 200 nL droplet contains 120 ng/mL αHL heptamer in buffer (10 mM MOPS, 1 M KCl, pH 7.0). Pores were incorporated into the bilayers at each droplet interface. Two Ag/AgCl electrodes connected to micromanipulators are inserted into droplets on the bottom left and top right corners of the network and connected to a patch-clamp amplifier to enable electrical recordings. Removal and insertion of these electrodes into other droplets is straightforward. (B) Current trace with an applied potential of −50 mV shortly after network formation. No blocking events are observed. (C) A central droplet (arrow) is removed and replaced with a 200 nL droplet containing 55 ng/mL αHL heptamer, 23 μM TRIMEB, and a small amount of tetramethylrhodamine (pink) in buffer. (D) Current trace with an applied potential of −50 mV shortly after the central droplet was replaced. Distinct types of blocking events are clearly observed: smaller blocking events that exhibit an "overshoot" of steady-state currents upon TRIMEB binding and dissociation (overshoot−overshoot) and larger blocking events that exhibit an "undershoot" of steady-state currents upon TRIMEB binding and dissociation (undershoot−undershoot).

further exploration. As the complexity of DIB networks increases, understanding and predicting their electrical behavior become more difficult. Thus, progress in the development of biologically relevant DIB networks requires a method to model and simulate their electrical properties. Such models can help explain and predict the behavior of DIB networks, as well as guide further experimentation.

The elements of a DIB network can be considered to be components of an electrical circuit in which bilayers serve as capacitors and incorporated αHL pores serve as resistors. We apply this modeling technique to thoroughly investigate a simple three-droplet network. Experimental measurements, theoretical analysis, and electrical circuit simulations of the current through the three-droplet network are in agreement, which validates our electrical circuit models. The intrinsic modularity and scalability of DIB networks should enable straightforward extension of the analysis presented in this paper to larger and more complex networks.

Results

Droplet Interface Bilayer Networks. The experimental platform used to create DIB networks consists of a Perspex chamber micromachined with an array of divots on the bottom surface (Figure S1). The chamber was filled with 10 mM 1,2-diphytanoyl-*sn*-glycero-3-phosphocholine in hexadecane. Aqueous droplets (200 nL) were submerged in the oil−lipid mixture and encased with lipid monolayers prior to network assembly (see Supporting Information). Electrodes were inserted into network droplets and connected to a patch-clamp amplifier to enable electrical measurements.

The construction of complex DIB networks that last for several days is simple and repeatable. For example, we created a 26-droplet "O−U" network in which all DIBs are interconnected by wild-type α-hemolysin (αHL) pores (Figure 1A). The electrical behavior of the network can be monitored by inserting Ag/AgCl electrodes into any two droplets (Figure 1A and B). It is possible to move the measurement electrodes to different parts of a network, allowing a complex network to be probed in sections or as a whole.

The behavior of DIB networks can be modified by extracting and inserting droplets of different compositions. For example, when the droplet between the "O" and "U" was replaced with a droplet containing both αHL and a reversible pore blocker, heptakis(2,3,6-tri-*O*-methyl)-β-cyclodextrin (TRI-

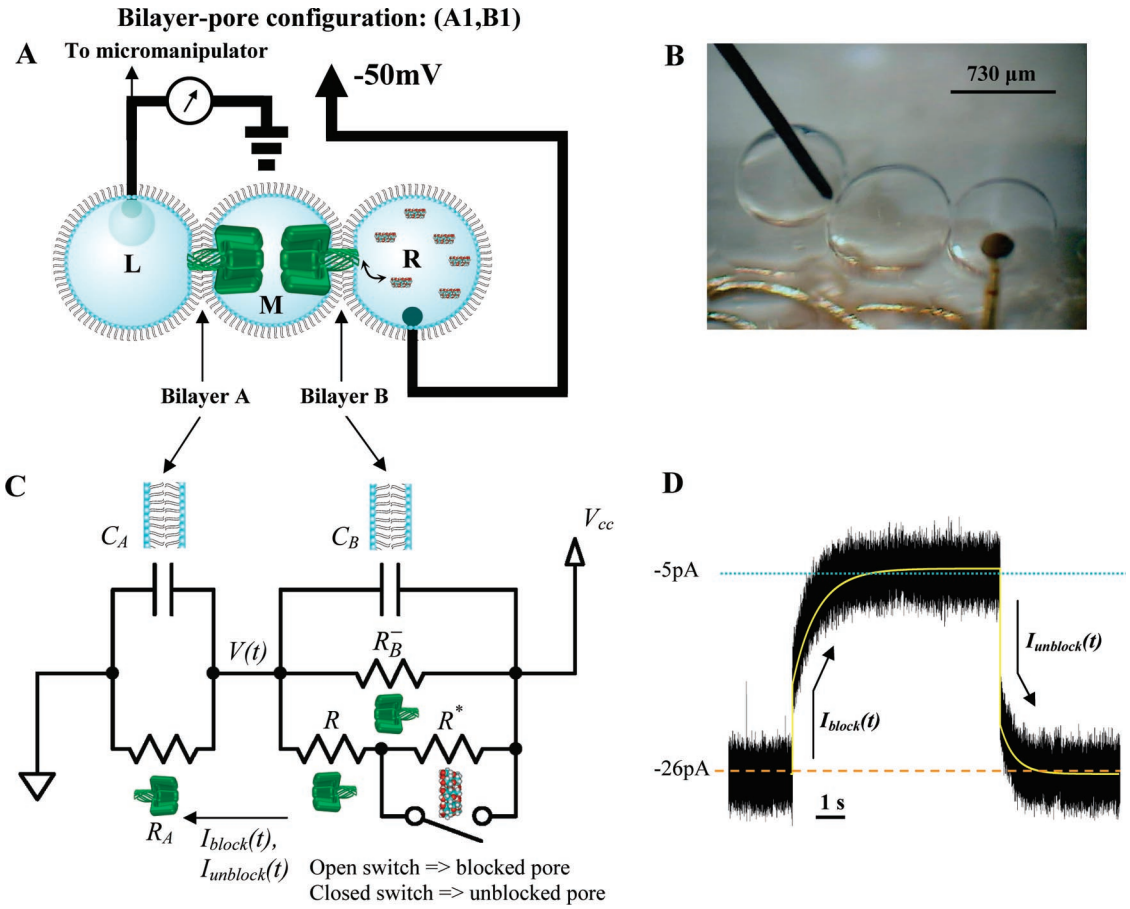

Figure 2. Double DIB experiments and analysis. (A) Setup for double DIB experiment. Droplet L contains buffer (10 mM MOPS, 1 M KCl, pH 7.0), M contains 1.7 ng/mL αHL heptamer in buffer, and R contains 10 μM TRIMEB in buffer. The potential is applied to droplet R, and droplet L is grounded. The current is measured from droplet R to droplet L. The pores insert into the two membranes with opposing orientations as shown. The bilayer−pore configuration illustrated is denoted (A1,B1). (B) Image of double DIB experimental setup with one moveable electrode and one fixed electrode. (C) Circuit schematic of double DIB system for analysis of blocking events in any bilayer−pore configuration. We assume that only one pore in bilayer B is blocked at a time. C_A is the capacitance and R_A is the net resistance of bilayer A (all pores in bilayer A combined). C_B is the capacitance of bilayer B, R_B^- is the net resistance of bilayer B excluding one pore (all pores in bilayer B combined except one that interacts with blocker), R represents a single pore in bilayer B that interacts with the blocker, and R^* represents the blocker that interacts with pore R. Opening the switch simulates the binding of the blocker to the pore, and closing the switch simulates the dissociation of the blocker from the pore. If there is only one pore in bilayer B, we simply set R_B^- to an infinite resistance. (D) Experimental current trace of a TRIMEB transient blocking event when the double DIB network is in bilayer−pore configuration (A1,B1). The applied voltage is −50 mV. Overlaid plot of theoretical current vs time (i.e., $I_{block}(t)$ and $I_{unblock}(t)$) during a TRIMEB blocking event for bilayer−pore configuration (A1,B1). The following parameter values are assigned (see text for details): $R_A = 0.9$ GΩ, $R = 1$ GΩ, $R_B^- = \infty$ (open), $R^* = 9$ GΩ, $C_A = 350$ pF, and $C_B = 500$ pF.

MEB; Figure 1C), blocking events in the current trace were evident (Figure 1D).

When TRIMEB binds or dissociates from an αHL pore in a single membrane system (Figure S2A), the current change is instantaneous because the voltage across the bilayer is constant (Figure S2B). This is manifested in the current trace as a square step. Moreover, all current blockade events have the same magnitude and shape.

In contrast, when TRIMEB binds or dissociates from an αHL pore in networks of two or more bilayers, the overall network current does not change to its new steady-state value instantaneously because the constant applied voltage is gradually redistributed among the bilayers in the network (Figure 1D). Furthermore, although the binding and dissociation of a TRIMEB molecule with an αHL pore is always the same physically and chemically, the effect on the network current depends on several factors, including bilayer areas, and pore location, quantity, distribution, and orientation. For example, when the central droplet of the "O−U" network contained TRIMEB (Figure 1C), the resulting current trace exhibited two types of blocking events (Figure 1D): (1) small amplitude events that exhibit an "overshoot" of the new steady-state currents when TRIMEB binds and dissociates from a pore, which we term "overshoot binding−overshoot dissociation," or "overshoot−overshoot" blocking events, and (2) large amplitude events that exhibit an "undershoot" of the new steady-state currents when TRIMEB binds and dissociates from a pore, which we term "undershoot binding−undershoot dissociation," or "undershoot−undershoot" blocking events.

Insights into the basis of DIB network behavior might be obtained from electrical circuit modeling. To demonstrate and validate our modeling approach, we compare experimental observations, electrical circuit simulation, and theoretical analysis of a simple three-droplet, double DIB network (Figure 2A) that can be viewed as a modular component of more complex networks (Figure 1). The simulation methods demonstrated can be applied to study other DIB networks as well.

Double DIB Network Experiments. We constructed a double DIB network with the L-droplet containing buffer (10 mM MOPS, 1 M KCl, pH 7.0), the M-droplet containing 1.7 ng/mL αHL heptamer in buffer, and the R-droplet containing 10 μM TRIMEB in buffer (Figure 2A and B). The notation (A*n*,B*m*) denotes the bilayer−pore configuration, where *n* and *m* are the number of αHL pores in bilayer A (L-M) and bilayer B (M-R), respectively (Figure 2A). For example, the bilayer−pore configuration (A3,B4) indicates that there are three pores in bilayer A and four pores in bilayer B.

Double DIB experiments ($n > 25$) were conducted with −50 mV applied to droplet R and droplet L grounded, which yielded negative current from droplet R to droplet L (Figure 2A). Unlike experiments with a single bilayer (Figure S2),[14,15] the current traces of blocking events in the double DIB network exhibit curvature (Figure 2D).

Net Current during Blocking Events in the Double DIB Network. In our experiments, current was observed only after there was at least one pore in each membrane: (A1,B1). This bilayer−pore configuration was easily recognized because it exhibits approximately half the current expected through a single pore. When TRIMEB binds to a single pore in bilayer B of the double DIB network in (A1,B1), there is an initial drop in current, followed by exponential decay toward the blocked steady-state current level (Figure 2D). TRIMEB dissociation is characterized by a sudden increase in current, followed by exponential decay toward the unblocked steady-state current level. We later describe a method for determining more complex bilayer−pore configurations in the section entitled "Spatial and Temporal Localization of Pore Insertions."

The analytical results that follow can be generalized to any blocker by modifying the blocker resistance in the model. The current through one αHL pore in a single-bilayer, two-droplet system at a voltage of −50 mV applied from β barrel to cap domain was −48 pA (Figure S2B), which is comparable to previous work.[14,15] The reversible TRIMEB binding reduced the pore current by ∼90% (Figure S2B). Based on this behavior, we create an electrical model in which each αHL pore is a resistor in parallel with a capacitor representing the bilayer (Figure 2C). The approximate resistance of a single αHL pore is (−50 mV)/(−48 pA) ≈ 1 GΩ (Figure S2B). The blocker is modeled as a resistor in series with αHL, and the reversible binding is represented by a switch (Figure 2C). Since TRIMEB blocks ∼90% of the current through αHL, we assign the blocker−pore complex a net resistance of 10 GΩ (i.e., pore, 1 GΩ; blocker, 9 GΩ). The capacitance of typical DIBs was ∼300 pF and could be reliably tuned between 150 and 600 pF by moving the droplets away from each other or pushing them closer together by adjusting the movable electrode(s). This observation is consistent with previously reported capacitance values for lipid bilayers[3,16] on the order of 10 fF/μm^2. The resistance of bilayers without inserted pores is on the order of 1 TΩ and can therefore be omitted from the model.

Since only droplet M contains protein (Figure 2A), and αHL pores insert into membranes with their β-barrel domain,[17] the cap domains of proteins inserting into both bilayers will remain in droplet M. Thus, the αHL pores in bilayers A and B will have opposing orientations. Using 1 M KCl, 10 mM MOPS, pH 7.0, we found that $I_{+50mV}/I_{-50mV} \approx 1.1$, which is comparable to previous results under similar conditions.[18] In other words, αHL conducts ∼1.1 times more current at 50 mV of applied potential when the current moves from β barrel to cap domain relative to the opposite polarity. Thus, to account for the rectification properties of αHL, we assign pores in bilayer A, $R_{bilayerA} = 50\text{ mV}/(1.1 \times 48\text{ pA}) \approx 0.9\text{ G}\Omega$, and pores in bilayer B, $R_{bilayerB} = -50\text{ mV}/-48\text{ pA} \approx 1\text{ G}\Omega$.

We derive analytical expressions for $I_{block}(t)$ and $I_{unblock}(t)$, the net current through the network as a function of time following binding and dissociation events, respectively (Figure 2C). We define the following electrical model parameters such that the analysis applies to any bilayer−pore configuration (Figure 2C). C_A and C_B represent bilayers A and B, respectively. V_{cc} is the applied voltage. All of the pores in bilayer A are combined into an equivalent resistor, R_A, which represents the net resistance of bilayer A (Figure 2C). Since a relatively low blocker concentration of 10 μM is used, we assume that only one pore in bilayer B is blocked at any given time. All of the pores in bilayer B except the one pore that interacts with the blocker are combined into the equivalent resistor R_B^- (Figure 2C). *R* represents the single pore that interacts with the blocker molecules, and R^* represents a single blocker molecule that binds to *R*. In reality, different pores in bilayer B get blocked at different times, but from a modeling perspective, this is not an issue because the resistances of all pores in bilayer B are assumed to be the same. Opening the switch simulates a blocker binding event, whereas closing the switch simulates a blocker dissociation event (Figure 2C). A table summarizing the symbols and abbreviations used in this paper is provided in the Supporting Information (Table S1).

Let

R_B = net resistance of bilayer B with all pores unblocked

R_B^* = net resistance of bilayer B with one pore blocked

$$R_B = R_B^- \,||\, R = \frac{RR_B^-}{R + R_B^-}$$

$$R_B^* = R_B^- \,||\, (R + R^*) = \frac{(R + R^*)R_B^-}{(R + R^*) + R_B^-}$$

[[$E \,||\, F \equiv$ the parallel combination of resistances E and F]]

Note that if there is only one pore in bilayer B, we set $R_B^- = \infty$, $R_B = R$, and $R_B^* = R + R^*$.

We first analyze the binding events. For $t < 0$, we assume that the switch is *closed* (Figure 2C, pore unblocked). Both capacitors will effectively be open circuits at $t = 0$. Hence, all of the current flows through the resistors, and the initial voltage at the middle node, $V(t)$, is

$$V(t = 0) = \left(\frac{R_A}{R_A + R_B}\right)V_{cc}$$

(14) Holden, M. A.; Bayley, H. *J. Am. Chem. Soc.* **2005**, *127*, 6502−6503.
(15) Holden, M. A.; Jayasinghe, L.; Daltrop, O.; Mason, A.; Bayley, H. *Nat. Chem. Biol.* **2006**, *2*, 314−318.
(16) Fettipla, R.; Andrews, D. M.; Haydon, D. A. *J. Membrane Biol.* **1971**, *5*, 277−296.
(17) Valeva, A.; Walev, I.; Pinkernell, M.; Walker, B.; Bayley, H.; Palmer, M.; Bhakdi, S. *Proc. Natl. Acad. Sci. U.S.A.* **1997**, *94*, 11607−11611.
(18) Miles, G.; Cheley, S.; Braha, O.; Bayley, H. *Biochemistry* **2001**, *40*, 8514−8522.

At $t = 0$, the switch opens to simulate the noncovalent binding of a blocker. We apply Kirchhoff's Current Law at the middle node to obtain

$$\frac{V_{cc} - V(t)}{R_B^*} + C_B \frac{d(V_{cc} - V(t))}{dt} = \frac{V(t)}{R_A} + C_A \frac{dV(t)}{dt}$$

The solution to this first-order homogeneous differential equation is

$$V(t) = \left[\frac{R_A}{R_A + R_B^*}\right]V_{cc} + \left[\frac{R_A}{R_A + R_B} - \frac{R_A}{R_A + R_B^*}\right]V_{cc} \times \exp\left(-\frac{R_A + R_B^*}{R_A R_B^*(C_A + C_B)}t\right)$$

The current through the network as a function of time is given by

$$I_{block}(t) = \alpha + \beta \exp(-\gamma t) \quad (1)$$

where

$$\alpha = \frac{V_{cc}}{R_A + R_B^*}$$

$$\beta = \frac{R_B^* - R_B}{R_B^*(R_A + R_B)(R_A + R_B^*)(C_A + C_B)} V_{cc}[R_B^* C_B - R_A C_A]$$

$$\gamma = \frac{R_A + R_B^*}{R_A R_B^*(C_A + C_B)}$$

Similarly, for the dissociation events,

$$\frac{dV(t)}{dt} + \frac{R_A + R_B}{R_A R_B(C_A + C_B)}V(t) = \frac{V_{cc}}{R_B(C_A + C_B)}$$

$$V(0) = \frac{R_A}{R_A + R_B^*}V_{cc}, \text{ and}$$

$$I_{unblock}(t) = \alpha' + \beta' \exp(-\gamma' t) \quad (2)$$

where

$$\alpha' = \frac{V_{cc}}{R_A + R_B}$$

$$\beta' = \frac{R_B^* - R_B}{R_B(R_A + R_B)(R_A + R_B^*)(C_A + C_B)} V_{cc}[R_A C_A - R_B C_B]$$

$$\gamma' = \frac{R_A + R_B}{R_A R_B(C_A + C_B)}$$

where $I_{unblock}(t)$ is the total current through the network as a function of time following dissociation. We have chosen $t = 0$ as the start of the dissociation event to simplify the expressions. Full mathematical derivations are provided in the Supporting Information.

To compare this analysis with the experimental trace of an (A1,B1) blocking event (Figure 2D), we assigned the following parameter values (Figure 2C): $R_A = 0.9$ GΩ, $R_B = 1$ GΩ ($R = 1$ GΩ, $R_B^- = \infty$), $R_B^* = 10$ GΩ ($R^* = 9$ GΩ). The experimental setup does not enable straightforward determination of the capacitance of each bilayer, only the net capacitance. However, it is possible to infer the bilayer capacitances by adjusting them in the model until the theoretical or simulated trace matches the experimental trace, while making sure that the net capacitance is in agreement with experimental measurements. By applying this strategy, we found that $C_A \approx 350$ pF and $C_B \approx 500$ pF (Figure 2C), which is reasonable because bilayer B is visibly larger than bilayer A (Figure 2B). The theoretical current vs time trace of a TRIMEB blocking event (Figure 2D, overlay created with Microsoft Excel) is similar to the experimental trace (Figure 2D).

Characteristics of Blocking Events in the Double DIB Network. The binding and dissociation current expressions in eqs 1 and 2 exhibit initial steps to $\alpha + \beta$ and $\alpha' + \beta'$, respectively, followed by an exponential decay toward steady-state current levels given by α and α', respectively. Depending on the signs of β and β', there are three possible types of behavior in the network current for both binding and dissociation: (1) "undershoot," (2) "exact," and (3) "overshoot." We define these terms as follows: the initial step in current (1) falls short of, i.e., undershoots, the new current level such that the step and decay occur in the same direction (Figure 3A, C, and D), (2) steps to the new steady-state current level exactly such that there is no subsequent decay phase, and (3) goes beyond, i.e., overshoots, the new steady-state current level such that the step and decay occur in opposite directions (Figure 3E, G, and H). Mathematically, the conditions for these three types of behavior are given by

$$V_{cc} < 0, \text{ so } \alpha, \alpha' < 0$$

Undershoot:

$\beta < 0$ requires that $R_A C_A < R_B^* C_B$ [[binding]]

$\beta' > 0$ requires that $R_A C_A < R_B C_B$ [[dissociation]]

Exact:

$\beta = 0$ requires that $R_A C_A = R_B^* C_B$ [[binding]] (3)

$\beta' = 0$ requires that $R_A C_A = R_B C_B$ [[dissociation]]

Overshoot:

$\beta > 0$ requires that $R_A C_A > R_B^* C_B$ [[binding]]

$\beta' < 0$ requires that $R_A C_A > R_B C_B$ [[dissociation]]

After the blocker binds, the potential across bilayer A decreases as C_A discharges, while the potential across bilayer B increases as C_B charges (Figure 2C). When the blocker dissociates, the reverse occurs. The *RC* time constant of each bilayer governs the rate at which it can charge or discharge. Thus, the net current will behave differently upon binding or dissociation depending on the relative magnitudes of the *RC* constants for the two bilayers as shown in eq 3. The binding and dissociation cases are not symmetrical

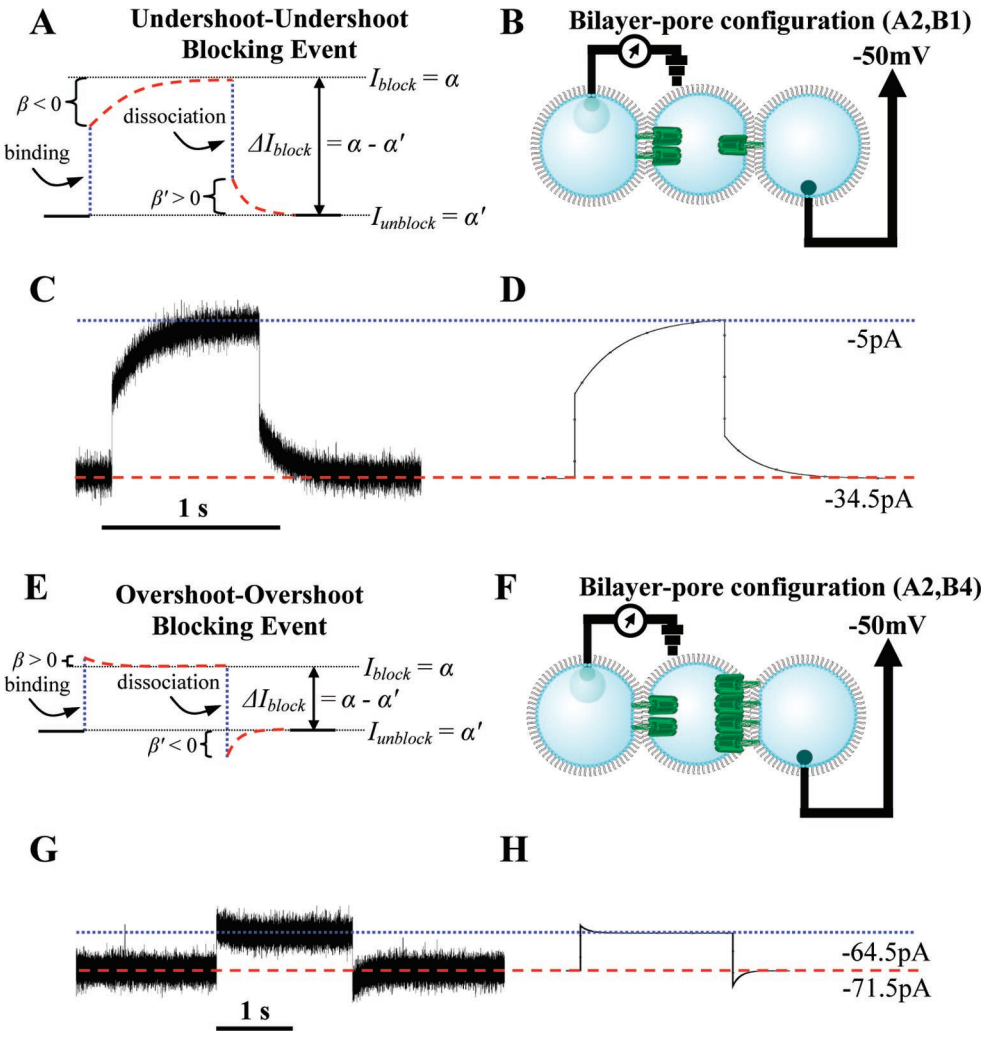

Figure 3. Types of blocking events in a double DIB network. (A) Diagram of undershoot−undershoot blocking event. Both the binding and dissociation consist of an undershoot phase (relative to the new steady-state current level) and an exponential decay phase. (B) Schematic of double DIB system in (A2,B1) bilayer−pore configuration. (C) Experimental current trace, and (D) simulated current trace of a TRIMEB undershoot−undershoot blocking event for bilayer−pore configuration (A2,B1). $C_A = C_B = 300$ pF. (E) Diagram of overshoot−overshoot blocking event. Both the binding and dissociation consist of an overshoot phase (relative to the new steady-state current level) and an exponential decay phase. (F) Schematic of double DIB system in (A2,B4) bilayer−pore configuration. (G) Experimental current trace, and (H) simulated current trace of a TRIMEB overshoot−overshoot blocking event for bilayer−pore configuration (A2,B4). $C_A = C_B = 300$ pF.

because the *RC* constant for binding includes the blocker resistance (i.e., R_B^*) whereas that for dissociation does not (i.e., R_B).

For simplicity, the rest of this section pertains to experiments where we set $C_A \approx C_B$, which allows us to neglect the capacitances present in eq 3. At a given steady-state unblocked current level, only one type of blocking event is observed. For example, eq 3 dictates that undershoot binding−undershoot dissociation, or undershoot−undershoot, type blocking events occur when $R_A < R_B$. For example, bilayer−pore configuration (A2,B1) yields undershoot−undershoot blocking events (Figure 3A, B, and C). Using SPICE (Simulation Program with Integrated Circuit Emphasis) to perform a time domain analysis of the equivalent circuit yields a similar trace (Figure 3D). On the other hand, overshoot−overshoot type blocking events occur when $R_A > R_B^*$ (Figure 3E). For bilayer−pore configuration (A2,B4) (Figure 3F), the experimental results (Figure 3G) and simulation results (Figure 3H) are again similar. Notice that these two types of current blocking events are the same as those seen in the "O−U" network (Figure 1). When $R_B^* > R_A > R_B$, e.g., (A2,B3), undershoot−overshoot blocking events are the result. Furthermore, the theoretical analysis predicts that it is not possible to observe overshoot−undershoot blocking events because $R_B < R_B^*$ by definition.

In actuality, DIBs also have series resistance from the buffer solution, which will have some effect on the resulting network current. The SPICE simulations show that changing the series resistance for each bilayer up to 100 kΩ has no significant effect on the results.

In agreement with the experimental data, the simulated magnitude (i.e., $\Delta\alpha = \alpha - \alpha'$) of undershoot−undershoot blocking events (Figure 3D) is generally larger than that of the overshoot−overshoot events (Figure 3H). The network tends toward undershoot−undershoot type events as pores are added to bilayer A and overshoot−overshoot type events as pores are added to bilayer B. The overshoot−overshoot blocking events are smaller because the blocking of a pore in membrane B becomes less significant when there are other open pores in the same membrane.

Generalizing Observed Experimental Trends Using Mathematical Analysis. An important advantage that theoretical analysis offers is the ability to verify or refute the generalizability

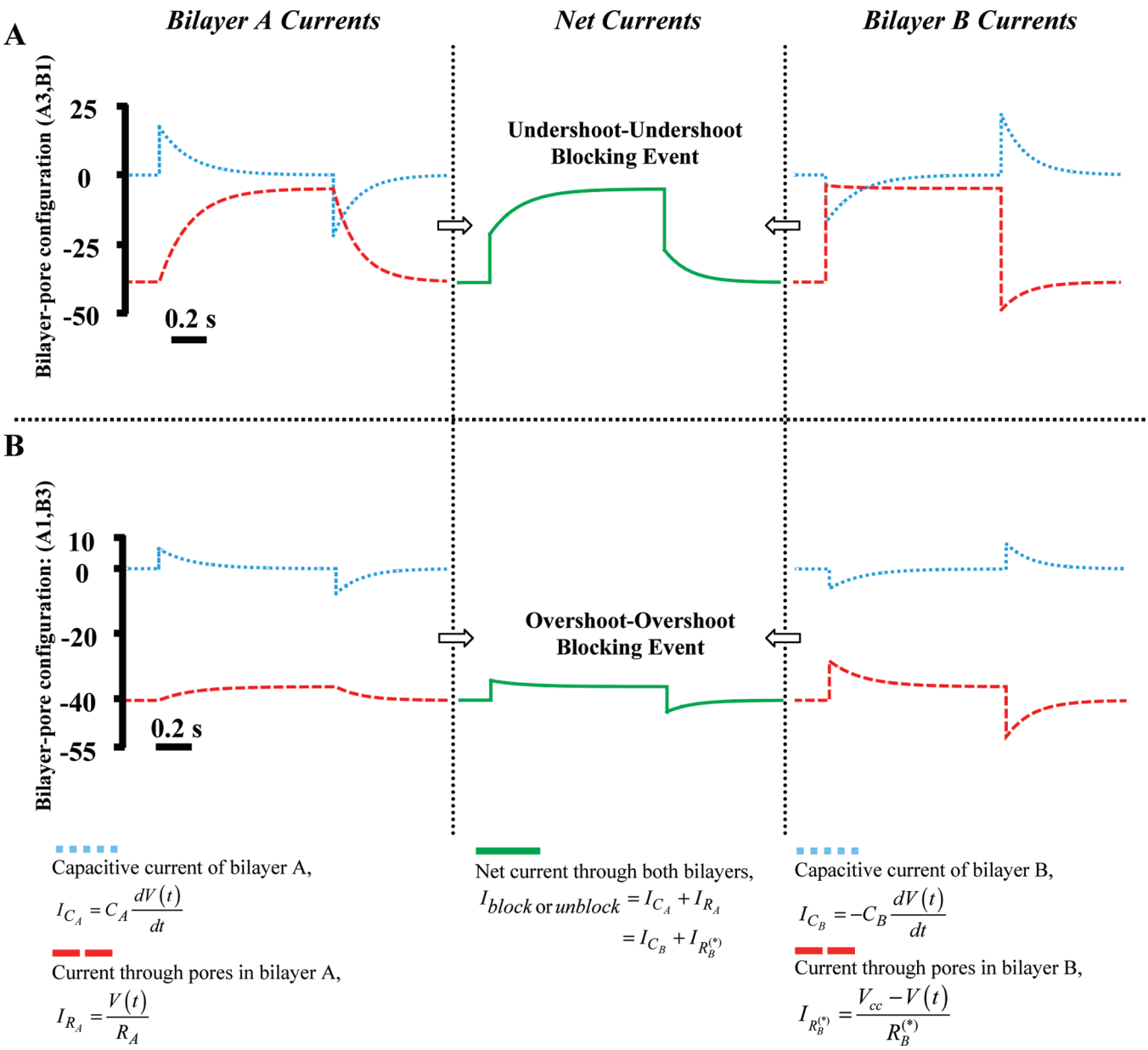

Figure 4. Separation of current during blocking events into components. SPICE was used to simulate a 1 s TRIMEB blocking event. The bilayer capacitances are $C_A = C_B = 300$ pF. The resistance of each pore in bilayer A is 0.9 GΩ, and that in bilayer B is 1 GΩ. The effective resistance of the blocker is 9 GΩ. The net current (solid lines, middle column) through the double DIB network can be separated into a capacitive current (dotted lines) and pore current (dashed lines) for each bilayer (bilayer A, left column; bilayer B, right column). By Kirchhoff's Current Law, the sum of the pore current and capacitive current for bilayer A and that for bilayer B both equal the net current through the network. Upon blocker binding, bilayer A discharges, bilayer B charges, and the pore currents for both bilayers decrease. Upon dissociation, bilayer A charges, bilayer B discharges, and the pore currents for both bilayers increase. (A) Bilayer−pore configuration (A3,B1) yields an undershoot−undershoot blocking event. (B) Bilayer−pore configuration (A1,B3) yields an overshoot−overshoot blocking event.

of observed experimental trends. For example, we observed that the initial step in current upon binding is smaller than that of dissociation (Figure 3C, D, G, and H). To determine whether this observation is true in general, we express it mathematically as

$$|(\alpha + \beta) - \alpha'| \stackrel{?}{<} |\alpha - (\alpha' + \beta')|$$

It is straightforward to show that this inequality holds (see Supporting Information), so the initial current step associated with dissociation is indeed greater than that of binding in all cases.

It was also experimentally observed that the decay rate for binding events is smaller than that of dissociation events. To determine if this is true in general, we note that eqs 1 and 2 tell us that the decay rates for binding and dissociation events are governed by γ and γ', respectively.

$$\frac{\gamma}{\gamma'} = \frac{R_A R_B + R_B R_B^*}{R_A R_B^* + R_B R_B^*}$$

since

$$R_B < R_B^*, \frac{\gamma}{\gamma'} < 1$$

$$\therefore \gamma < \gamma'$$

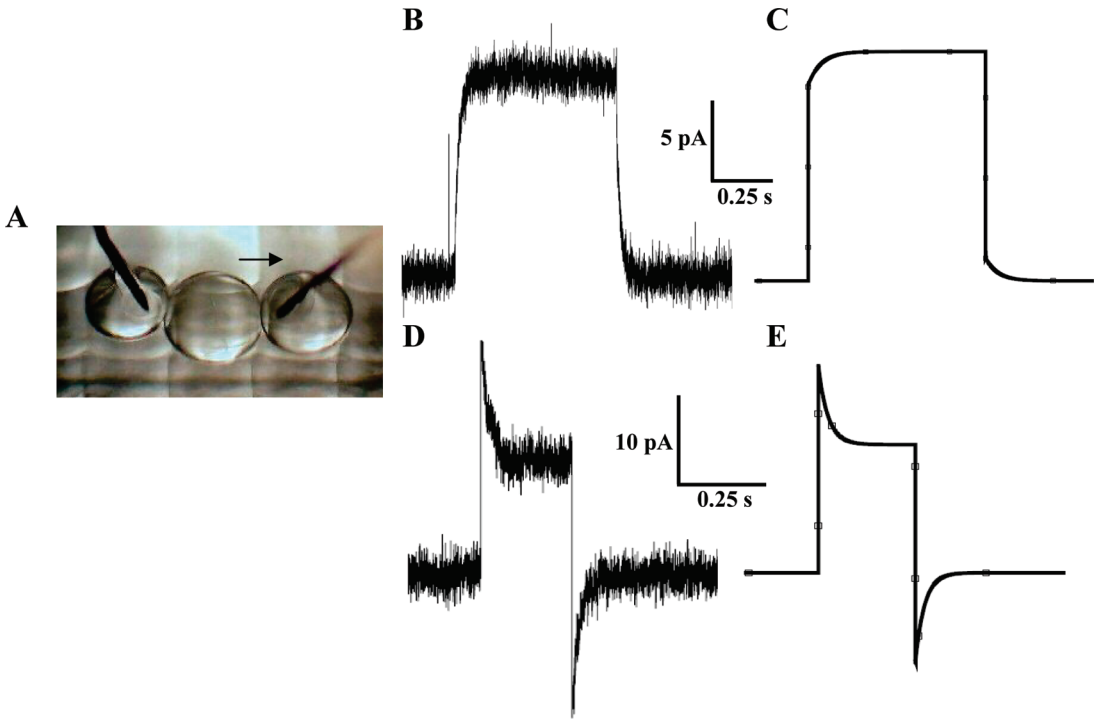

Figure 5. Effects of bilayer capacitance on blocking event characteristics. (A) Double DIB setup with two movable electrodes. Left droplet contains buffer (10 mM MOPS, 1 M KCl, pH 7.0), middle droplet contains 1.7 ng/mL αHL heptamer in buffer, and right droplet contains 10 μM TRIMEB in buffer. The potential (−50 mV) is applied to the right droplet, and the left droplet is grounded. (B) Experimental current trace of blocking event in bilayer−pore configuration (A9,B8). (C) Simulated current trace of blocking event in bilayer−pore configuration (A9,B8) with C_A = 400 pF and C_B = 400 pF. (D) Bilayer B (droplets M and R) was reduced in size by moving the right electrode to the right as indicated by the arrow in part A. Over 90 s, bilayer B gradually shrank until droplets M and R separated. The experimental current trace of a blocking event in bilayer−pore configuration (A9,B8) immediately before bilayer B separated is shown. (E) Simulated current trace of blocking event in bilayer−pore configuration (A9,B8) with C_A = 400 pF and C_B = 25 pF.

Thus, the exponential decay rate for dissociation is greater than that of binding in all cases.

Separation of Current during Blocking Events into Components. One of the most useful features of SPICE simulations is the ability to probe the voltage at any node and the current through any element in the network as a function of time. Experimentally, this would be equivalent to plugging the electrodes into different droplets in the network. However, such an action would be undesirable with the present setup because it would fundamentally change the circuit since the same electrodes provide the voltage-clamp and measurement capabilities.

As required by Kirchhoff's Current Law and shown in eqs 1 and 2, the sum of the capacitive current (I_{C_A}) and the pore current (I_{R_A}) for bilayer A (Figure 4, *left column*) must equal the net current through the entire network (Figure 4, *middle column*). This must also be the case for bilayer B (Figure 4, *right column*). This fundamental property can be verified with SPICE simulations for all types of blocking events, including undershoot−undershoot (Figure 4A) and overshoot−overshoot (Figure 4B). Notice that the capacitive currents are opposite in direction and equal in magnitude when $C_A = C_B$ (Figure 4). Moreover, the pore current through bilayer A is continuous whereas that through bilayer B is discontinuous (Figure 4).

Effects of Bilayer Capacitance on Blocking Event Characteristics. Unlike the case with planar bilayers, it is possible to change the capacitance of DIBs during an experiment.[2] A dual movable electrode setup (Figure 5A) enabled us to modulate the capacitance of one bilayer with minimal perturbation of the other. The experimental and simulated TRIMEB blocking events seen in bilayer−pore configuration (A9,B8) displayed undershoot−undershoot characteristics (Figure 5B and C). The capacitance of both bilayers was ∼400 pF. The capacitance of bilayer B was then reduced by moving the corresponding electrode to the right (Figure 5A, arrow). Bilayer B gradually shrank over the span of 90 s, and the characteristics of the blocking events changed accordingly while the bilayer−pore configuration remained (A9,B8). Immediately prior to bilayer B separation, the blocking events began displaying overshoot−overshoot characteristics (Figure 5D and E) as predicted by eq 3. These results demonstrate that both bilayer resistances and capacitances are important in determining the characteristics of blocking events and that a physical change to the DIB network can alter the overall electrical behavior.

Net Current during Pore Insertions in the Double DIB Network. Unlike the single DIB case, where the insertion of each additional pore is characterized by a current step of the same magnitude (Figure 6A), current steps are variable in the double DIB network (Figure 6B). We simulated pore insertions in double DIB networks with an analysis similar to that presented for blocking events. To model a pore insertion into bilayer A, we add a resistor, R, in parallel with the net bilayer resistance, R_A^-, at $t = 0$ by closing the switch (Figure 6C). The net resistance of bilayer A after pore insertion is $R_A = R \,||\, R_A^- = RR_A^-/(R + R_A^-)$. The net resistance of bilayer B is R_B, and the

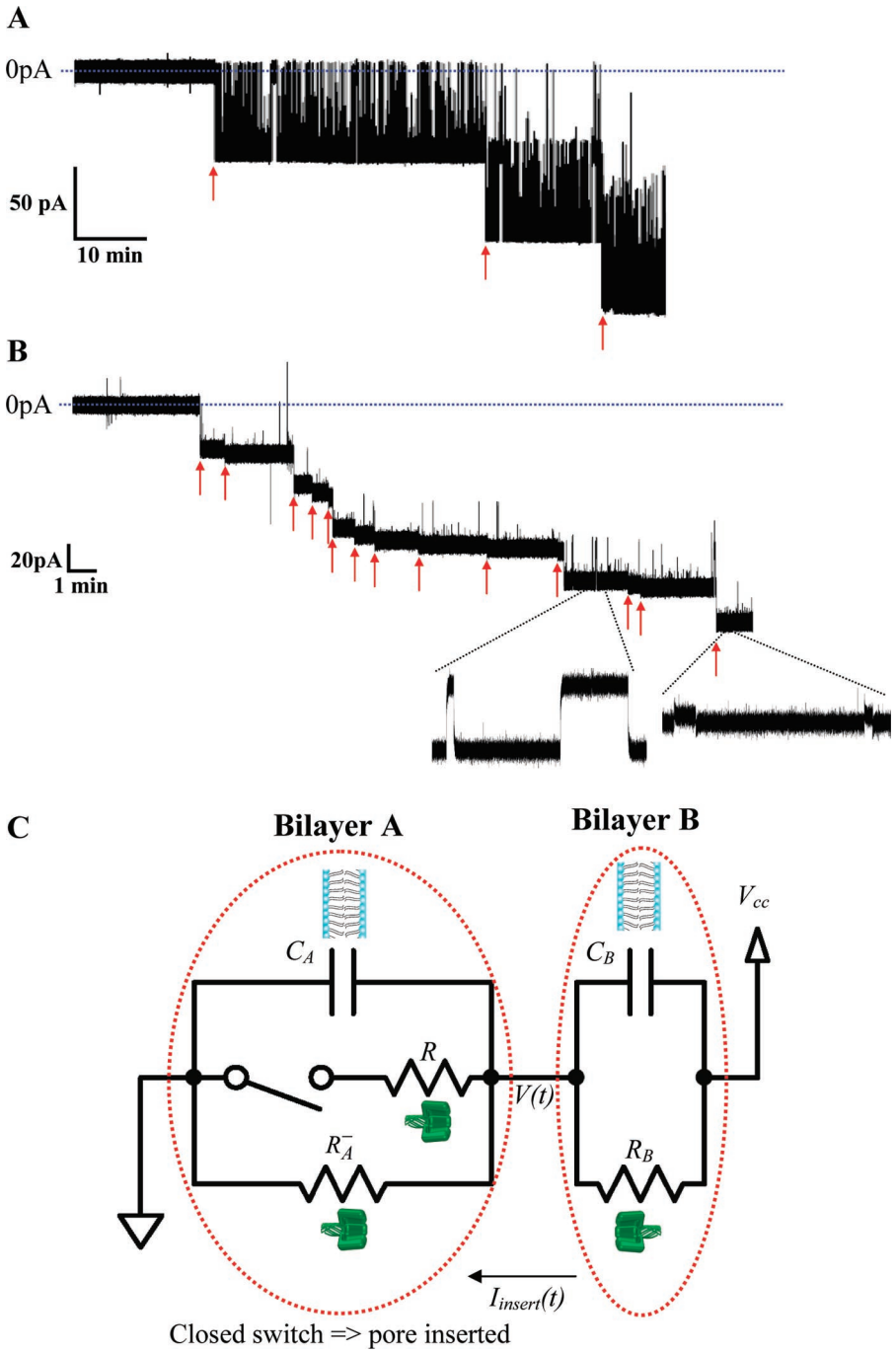

Figure 6. Pore insertions in single DIB and double DIB experiments. (A) Experimental current trace during pore insertions in a single DIB system with TRIMEB blocking events. Droplet contents are described in Figure S2. The current steps and blocking events are uniform in size. Pore insertions are marked with arrows. (B) Experimental current trace during pore insertions in a double DIB system with TRIMEB blocking events. Droplet contents are described in Figure 2. The current steps and blocking events exhibit a range of sizes. Two regions of the trace illustrating different types of blocking events are expanded for clarity. (C) Circuit schematic of double DIB system for analysis of pore insertions. C_A is the capacitance of bilayer A, R_A^- is the net resistance of bilayer A before pore insertion, and C_B and R_B are the capacitance and net resistance of bilayer B, respectively. A new pore, R, is inserted into bilayer A by closing the switch.

capacitances of bilayers A and B are C_A and C_B, respectively. Since the switch was open for $t < 0$, the initial condition is $V(t = 0) = R_A^- V_{cc}/(R_A^- + R_B)$.

Applying Kirchhoff's Current Law to the middle node,

$$\frac{V_{cc} - V(t)}{R_B} + C_B \frac{d(V_{cc} - V(t))}{dt} = \frac{V(t)}{R_A} + C_A \frac{dV(t)}{dt}$$

The solution for $V(t)$ is

$$V(t) = \left[\frac{R_A}{R_A + R_B}\right] V_{cc} + \left[\frac{R_A^-}{R_A^- + R_B} - \frac{R_A}{R_A + R_B}\right] V_{cc} \times \exp\left(-\frac{R_A + R_B}{R_A R_B (C_A + C_B)} t\right)$$

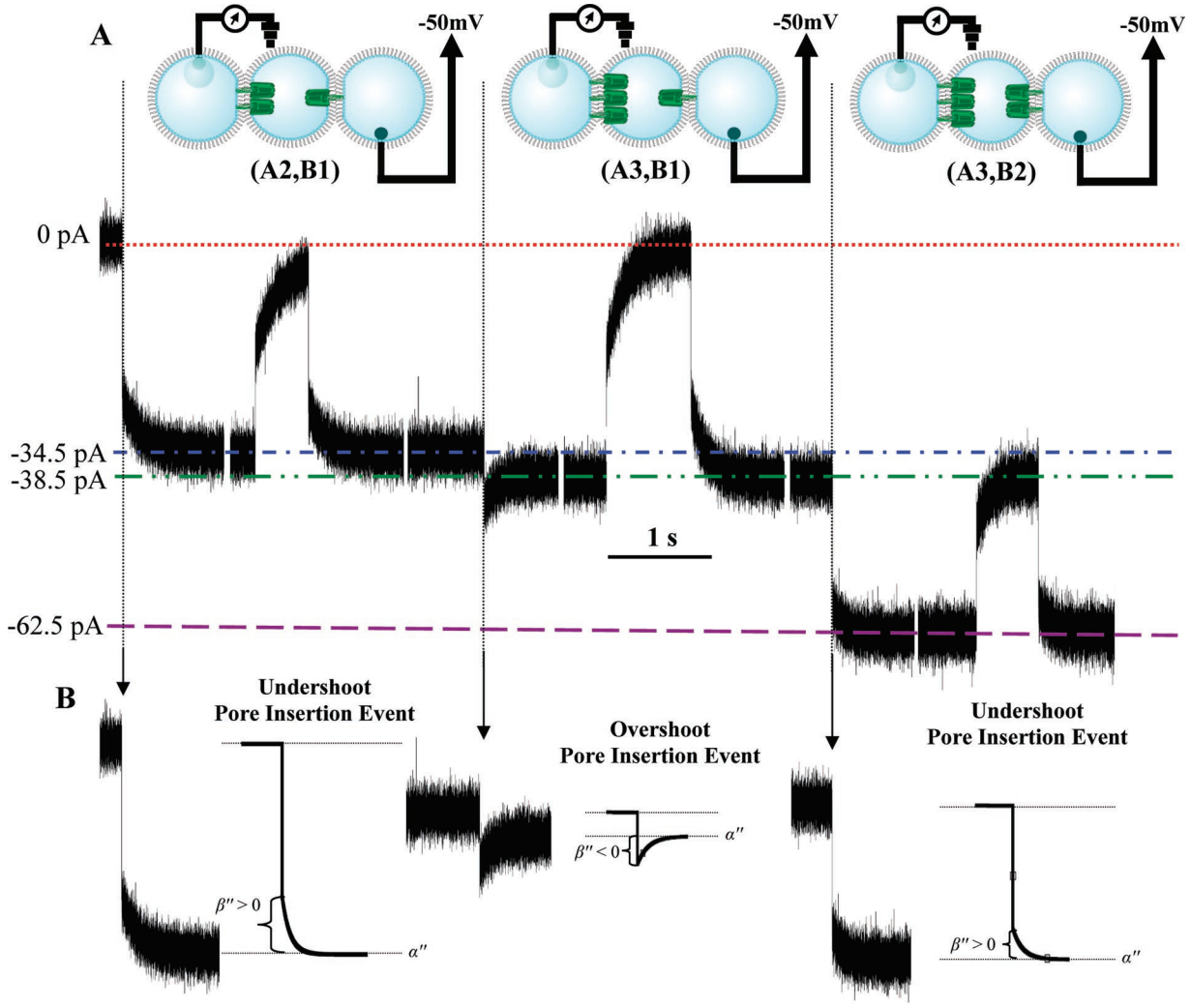

Figure 7. Spatial and temporal localization of pore insertions. (*A*) Current trace from one double DIB experiment illustrating (A2,B0) → (A2,B1) → (A3,B1) → (A3,B2) pore insertions. Droplet contents are described in Figure 2. The trace is presented as six segments separated by gaps to save space. Only one blocking event at each current level is shown. Horizontal lines indicate the current levels for 0 pA and (A2,B1), (A3,B1), and (A3,B2), respectively. Pore insertions are indicated by vertical dotted lines. (B) Simulated current traces of (A2,B0) → (A2,B1), (A2,B1) → (A3,B1), and (A3,B1) → (A3,B2) pore insertions juxtaposed with corresponding segments of the experimental traces. $C_A = C_B = 300$ pF. $R = 0.9$ GΩ for insertions into bilayer A, and $R = 1$ GΩ for insertions into bilayer B.

The current through the network as a function of time is given by

$$I_{\text{insert}}(t) = \alpha'' + \beta'' \exp(-\gamma'' t) \tag{4}$$

where

$$\alpha'' = \frac{V_{cc}}{R_A + R_B} = \alpha'$$

$$\beta'' = \frac{(R_A C_A - R_B C_B)(R_A - R_A^-)}{R_A(R_A + R_B)(R_A^- + R_B)(C_A + C_B)} V_{cc}$$

$$\gamma'' = \frac{R_A + R_B}{R_A R_B (C_A + C_B)} = \gamma'$$

Note that the steady-state current after a pore insertion (α'') is the same as that after dissociation of a blocker (α') when both events occur with the same final bilayer−pore configuration.

Characteristics of Pore Insertions in the Double DIB Network. Depending on the sign of β'', there are three possible types of behavior in the network current upon insertion of an additional pore (Figure 7B): (1) "undershoot," (2) "exact," and (3) "overshoot." These terms are defined as before. Mathematically, the conditions for these three types of behavior are given by

$$V_{cc} < 0, \text{ so } \alpha'' < 0$$

Undershoot:

$$\beta'' > 0 \text{ requires that } (R_A C_A - R_B C_B)(R_A - R_A^-) < 0$$

Exact: (5)

$$\beta'' = 0 \text{ requires that } (R_A C_A - R_B C_B)(R_A - R_A^-) = 0$$

Overshoot:

$$\beta'' < 0 \text{ requires that } (R_A C_A - R_B C_B)(R_A - R_A^-) > 0$$

The above conditions can be generalized to the situation where the new pore inserts into bilayer B by replacing all "A"

subscripts with "B" and vice versa. Note that R takes on a different value depending on which bilayer the pore inserts into because of the rectification properties of αHL.[18]

Spatial and Temporal Localization of Pore Insertions. Although pores and channels in droplets will continue to insert into DIBs for some time after network creation, the approximate number of pores and channels in a given DIB can be controlled by adjusting the dilution of the protein. By analyzing three key features of current traces obtained from double DIB experiments, we can determine when and where each new pore inserts during an experiment (Figure 7A). First, because of the rectification properties of αHL, the steady-state unblocked current level (α') given by eq 2 indicates the bilayer−pore configuration, although it is theoretically possible for more than one bilayer−pore configuration to have the same α'. Second, the nature of the current increase induced by a pore insertion will depend on the bilayer−pore configurations before and after the insertion event as shown by eq 4. Third, the characteristics of blocking events also indicate the bilayer−pore configuration.

We demonstrate spatial and temporal localization of pore insertions in a single experiment (Figure 7A). The first current step of $\alpha' \approx -34.5$ pA shows that the configuration of pores is (A2,B1). This current step corresponds to pore insertion into bilayer B. If the configuration is (A1,B2) instead, then $\alpha' \approx -36$ pA. The difference in steady-state current between (A2,-B1) and (A1,B2) is a result of the rectification properties of αHL. Further confirmation comes from examining a blocking event at this current level. The large (∼30 pA) undershoot−undershoot blocking event establishes the bilayer−pore configuration is (A2,B1). If the configuration is (A1,B2) instead, eq 3 reveals that we would observe undershoot−overshoot blocking events because $R_B < R_A < R_B^*$. Thus, we conclude that the first transition observed in the current trace must be (A2,B0) → (A2,B1).

For the second pore insertion, both the new unblocked steady-state current level of −38.5 pA and the characteristics of the blocking events suggest that the bilayer−pore configuration is (A3,B1) and not (A2,B2). However, in this case, the most direct method of determining where the pore inserted is to examine the characteristics of the pore insertion itself. An overshoot-type pore insertion event is observed (Figure 7); if the insertion occurred in bilayer B instead, an undershoot-type pore insertion event would be expected. Therefore, the second transition is (A2,B1) → (A3,B1). The same method can be applied to the third pore insertion (Figure 7) to yield (A3,B1) → (A3,B2).

Discussion

The electrical behavior of a network of bilayers with incorporated pores differs dramatically from that of single bilayer systems (Figure 1). For example, in DIB networks, the same physical and chemical interaction of a reversible pore blocker such as TRIMEB with an αHL pore can have distinctly different effects on the network current depending on several factors such as bilayer−pore configuration and bilayer areas. To investigate the basis for these differences, we used electrical circuit analysis and SPICE simulations to analyze protein pore insertion and blockade in a simple three-droplet, two-bilayer network. Our analysis provides explicit mathematical relationships that specify the conditions under which each type of pore blocking or insertion event is expected to occur. In fact, our analysis of the three-droplet network enables us to understand the electrical phenomena seen in more complex networks, such as the "O−U" system (compare Figure 1D with Figure 3).

The experimental methods do not directly enable the determination of how many pores are in each of the two membranes since the electrodes are separated by two bilayers. However, we showed that SPICE simulation offers a rapid method of exploring pore distributions between the two bilayers. The synergy of experiment, theory, and simulation enabled the determination of when and where each successive pore inserts. We have shown that the events at one interface (e.g., current blockades) can provide information about phenomena (e.g., pore insertions) at another bilayer in the network.

Pores and channels that exhibit a variety of conductance, ion selectivity, rectification, gating, and blocker interaction properties provide a toolbox for developing more elaborate DIB networks. Genetically engineered αHL pores can be tailored to provide a range of specific functions, including specific blocker affinities, ion selectivities, rectification, and chemical reactivity.[12,19−23] As networks become more complex, simulations will be critical for predicting and understanding network behavior. Therefore, the present analysis of a simple DIB network will be instrumental in the development of larger, functional networks. Complex networks can be treated as modular arrangements of simpler systems, such as the three-droplet network.

The ability to form networks of "protocells" that communicate through membrane proteins forms a basis for the development of an artificial platform for studying multicellular biological systems.[24,25] For example, electrically propagating systems, such as the heart, might be mimicked by DIB networks containing channels found in cardiac tissue. This may allow us to simulate and study the properties and mechanisms of electrical impulse propagation, as well as the fundamental underpinnings of pathological behavior.[26]

Acknowledgment. The authors thank Dr. Mark Wallace (University of Oxford) and Professor Michael Gustafson (Duke University) for helpful discussions. The α-hemolysin heptamers were prepared by Ellina Mikhailova and Qiuhong Li. William L. Hwang is an American Rhodes Scholar. Professor Hagan Bayley is the holder of a Royal Society-Wolfson Research Merit Award. This work was supported by a grant from the Medical Research Council.

Supporting Information Available: Experimental details, mathematical derivations, figures illustrating the procedure for constructing droplet interface bilayer networks and electrical current traces for a single αHL pore, and a table summarizing the abbreviations and mathematical symbols used throughout the paper. This material is available free of charge via the Internet at http://pubs.acs.org.

JA074071A

(19) Gu, L. Q.; Cheley, S.; Bayley, H. *J. Gen. Physiol.* **2001**, *118*, 481−493.
(20) Gu, L. Q.; Dalla Serra, M.; Vincent, J. B.; Vigh, G.; Cheley, S.; Braha, O.; Bayley, H. *Proc. Natl. Acad. Sci. U.S.A.* **2000**, *97*, 3959−3964.
(21) Bayley, H.; Cremer, P. S. *Nature* **2001**, *413*, 226−230.
(22) Gu, L. Q.; Cheley, S.; Bayley, H. *Science* **2001**, *291*, 636−640.
(23) Gu, L. Q.; Braha, O.; Conlan, S.; Cheley, S.; Bayley, H. *Nature* **1999**, *398*, 686−690.
(24) Basu, S.; Mehreja, R.; Thiberge, S.; Chen, M. T.; Weiss, R. *Proc. Natl. Acad. Sci. U.S.A.* **2004**, *101*, 6355−6360.
(25) Chen, M. T.; Weiss, R. *Nat. Biotechnol.* **2005**, *23*, 1551−1555.
(26) Kleber, A. G.; Rudy, Y. *Physiol. Rev.* **2004**, *84*, 431−488.